PNAS
www.pnas.org

Supplementary Information for

The optoelectronic microrobot: A versatile toolbox for micromanipulation

Shuailong Zhang[1,2,3], Erica Y. Scott[1,2,3], Jastaranpreet Singh[1,3], Yujie Chen[4], Yanfeng Zhang[4], Mohamed Elsayed[1,3], M. Dean Chamberlain[1,2,3], Nika Shakiba[1,3], Kelsey Adams[1,5], Siyuan Yu[4,6], Cindi M. Morshead[1,3,5,7], Peter W. Zandstra[1,3,8,9,10] and Aaron R. Wheeler[1,2,3,*]

1. *Donnelly Centre for Cellular and Biomolecular Research, University of Toronto, Toronto, ON, Canada M5S 3E1*
2. *Department of Chemistry, University of Toronto, Toronto, ON, Canada M5S 3H6*
3. *Institute for Biomaterials and Biomedical Engineering, University of Toronto, Toronto, ON, Canada M5S 3G9*
4. *State Key Laboratory of Optoelectronic Materials and Technologies, School of Electronics and Information Technology, Sun Yat-sen University, Guangzhou 510275, China*
5. *Institute of Medical Sciences, University of Toronto, Toronto, ON, Canada, M5S 1A8*
6. *Photonics Group, Merchant Venturers School of Engineering, University of Bristol, Bristol BS8 1UB, United Kingdom*
7. *Department of Surgery, University of Toronto, Toronto, ON, Canada, M5T 1P5*
8. *School of Biomedical Engineering, University of British Columbia, Vancouver, BC, Canada V6T 1Z3*
9. *The Biomedical Research Centre, University of British Columbia, Vancouver, BC, Canada, V6T 1Z3*
10. *Michael Smith Laboratories, University of British Columbia, Vancouver, BC, Canada V6T 1Z4*

Correspondence: Aaron R. Wheeler, Email: aaron.wheeler@utoronto.ca

This Appendix includes:

Other supplementary materials for this manuscript include the following:

Movies S1-S9

www.pnas.org/cgi/doi/10.1073/pnas.1903406116

1. Calculation of manipulation force responsible for bead/cell motion

In this work, the Reynolds number for a 15-μm-diameter polystyrene bead moved by the microrobot at a maximum linear velocity of 912 μm/s is 0.0154, suggesting that the system is in the laminar flow regime. This verifies an important experimental assumption: the low inertial forces allow the estimation of manipulation force responsible for bead motion to be equivalent to the viscous drag force, which is given by Stoke's law,[1-5]

$$F_{manipulation} = F_{viscous\_drag} \quad (1)$$

$$F_{viscous\_drag} = 6\pi\eta r v \quad (2)$$

where η is the viscosity of the liquid, r is the radius of the bead and v is velocity of the bead. Since in these experiments gravity forces the bead to settle in proximity to the device surface, Faxen's correction was used to adjust the calculation of viscous drag force,[1-5]

$$F_{vicious\_drag} = \frac{6\pi\eta r v}{\left(1-\frac{9}{16}\left(\frac{r}{h}\right)+\frac{1}{8}\left(\frac{r}{h}\right)^3-\frac{45}{256}\left(\frac{r}{h}\right)^4-\frac{1}{16}\left(\frac{r}{h}\right)^5\right)} \quad (3)$$

where h is the distance from the surface to the center of the bead. Thus, the manipulation forces reported in the main text were calculated using Equations (1)-(3).

2. Exploration of microrobot height and material

Cogwheel-shaped microrobots with different heights were fabricated as described in the main text, with heights verified using an optical Profilometer (Bruker Contour GT-K). Maximum linear translation velocities as a function of bias voltatge are shown in Fig. S1*A*.

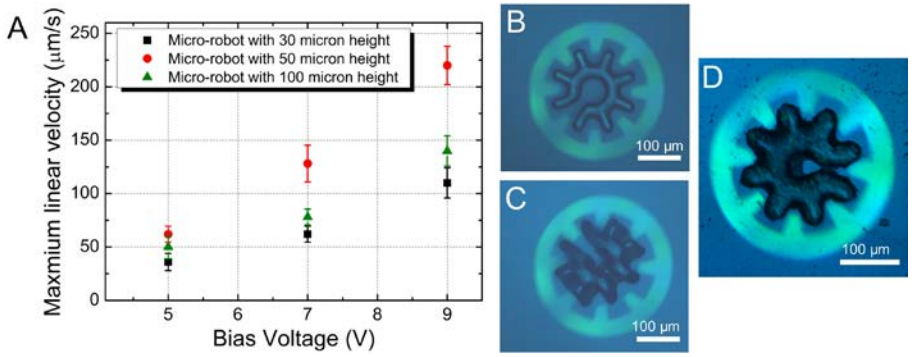

Fig. S1. Microrobots with different heights and materials. (*A*) Maximum linear velocities of cogwheel-shaped microrobots with hights of 30 μm (black aquares), 50 μm (red circles), or 100 μm (green triangles) as a function of bias voltage. Error bars represent ±1 standard deviation from five measurements for each condition. Bright-field images of a cogwheel-shaped microrobot with 30 μm height (*B*) before and (*C*) after flipping on its edge during linear translation. (*D*) Bright-field image of a cogwheel-shaped microrobot formed from silver-nanoparticle-doped SU-8 during linear translation.

As shown, the maximum linear velocities for robots with heights of 30, 50, and 100 μm are 110, 220, and 140 μm/s, respectively, when driven at 9 $V_{p\text{-}p}$ at 20 kHz. Microrobots with small heights were the least stable, often observed to flip vertically to form a "Stonehenge"-like structure during the manipulation process (Fig. S1*B*

and *C*). Microrobots with large heights were observed to move slugglishly, limited by the increased drag for these larger structures (relative to thinner microrobots). Finally, microrobots formed from SU-8 doped with silver nanoparticles were formed and manipulated (Fig. S1*D*), with maximum velocities and other behaviour similar to those formed from un-altered SU-8.

3. Numerical simulations

3D simulations of the cogwheel-shaped OET trap were generated in COMSOL Multiphysics using the AC/DC module (COMSOL Inc., Burlington, MA, accessed via license obtained through CMC Microsystems, Kingston, Canada). The AC/DC module uses the quasi-static approximation which assumes that the wavelength of applied AC signal is much larger than the dimensions of the simulation model. This assumption is justified for the model shown in Fig. 1*N* in the main text, as the wavelength of the applied AC signal is 6×10^3 m and the critical dimensions are 500 μm across X and Y planes and 150 μm across Z plane. The boundary conditions were set to perfect electrical insulation at the sides and continuity for all interior boundaries. Initial electric potential was set to 0 V for all domains. The top surface was set to 0 V and the bottom surface was set to 20 V to simulate the applied AC signal (frequency set to 25 kHz). The model included a 1-μm-thick a-Si:H layer at the bottom and a 149-μm-thick liquid chamber. The conductivities σ and permittivities ε were set to $\sigma_{silicon\text{-}light}$ = 1×10^{-4} S/m, $\sigma_{silicon\text{-}dark}$ =1×10^{-6} S/m, $\varepsilon_{silicon}$ = 11.7, σ_{medium} =5×10^{-3} S/m, and ε_{medium} =80. The model employed a free tetrahedral mesh with a maximum element size of 25 μm, a minimum element size of 0.3 μm, a maximum element growth rate of 1.35, a curvature factor of 0.4, and a resolution of narrow regions of 0.85.

4. Cell viability assay

Suspensions of ARPE-19 and MCF-7 cells in sucrose media were prepared as described in the main text, except without labeling with CellTracker dye. The suspension media contained 3 μM Propidium Iodide (PI), formed by diluting a stock 1.5 mM PI solution from Invitrogen 1 to 500 in sucrose buffer. Cells were loaded in OET devices with and without cogwheel-shaped microrobots as described in the main text. Four conditions were evaluated: ARPE-19 cells or MCF-7 cells manipulated with OET-alone, and ARPE-19 cells or MCF-7 cells manipulated with microrobots. In all cases, the light pattern used to manipulate cogwheel-shaped microrobots was projected and a 7 $V_{p\text{-}p}$ bias voltage (at 20 kHz) was applied. The optical power density of the projected light pattern was measured to be 0.84 W/cm^2. In OET-alone experiments (conducted in 10 different OET devices for each cell type), the light pattern was used directly to trap five live cells and translate them at 15 μm/s for 100 seconds across a distance of 1.5 mm. After this, the number of dead cells were determined on the basis of their red fluorescence (derived from PI). The results of two such experiments are shown in Fig. S2. Specifically, Fig. S2*A-C* depicts a group of five APRE-19 cells and Fig. S2*D-F* depicts a group of five MCF-7 cells before, during, and after being manipulated. In both cases, one of the five cells died (as indicated by the PI stain). In the microrobot experiments (conducted in 10 different OET devices for each cell type), a microrobot was used to load two-to-five live cells into the robot (depending on the sizes of the selected cells), which was then used to translate them at 15 μms for 100 seconds across a distance of 1.5 mm. The results were tabulated as above, with a representative experiment shown in Fig. S2*G-I*. At the conclusion of all experiments, the total numbers of live

cells (prior to translation) and the numbers of dead cells (after translation) were summed across all replicates and reported as % viability in the main text (Fig. 3*J*).

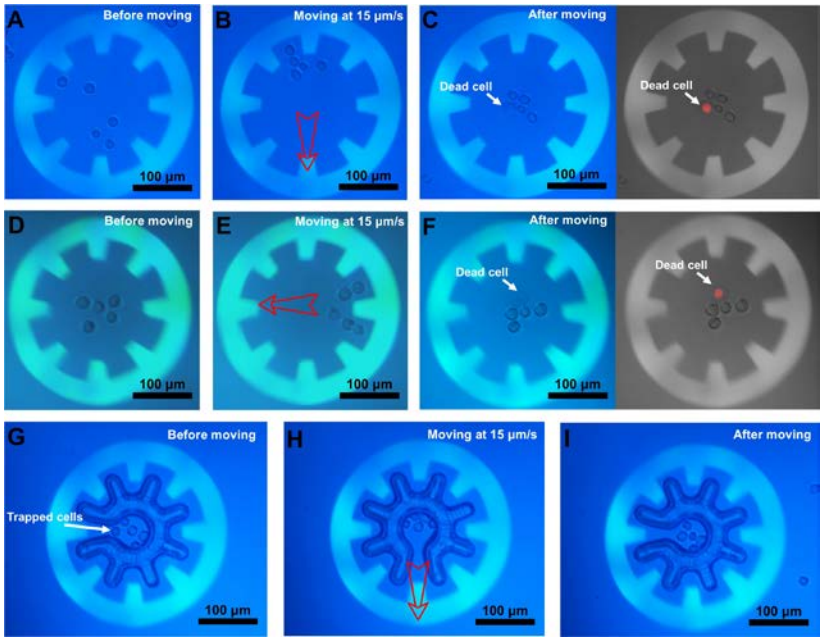

Fig. S2. Cell viability assay. Representative micrographs of five cells collected before (*A*, *D*, *G*) during (*B*, *E*, *H*), and after (*C*, *F*, *I*) translation by OET alone (*A*-*F*) or in a cogwheel-shaped microrobot (*G*-*I*). The cells in each image are APRE-19 (*A*-*C*, *G*-*I*) or MCF-7 (*D*-*F*). Most images are bright-field (*A*, *B*, *C*-left, *D*, *E*, *F*-left, and *G*-*I*); two are fluorescent (*C*-right, *F*-right), in which the red-color indicates fluorescence from propidium iodide. Open red arrows indicate the direction of translation. Scale bars are 100 µm.

5. Micro-well devices for clonal expansion and RNA-seq

OET devices used for clonal expansion and RNA-seq were formed as described in the main text, except that the bottom plate (bearing the a-Si:H layer) was first modified (in the Center for Microfluidic Systems cleanroom facility at the University of Toronto) to bear an array of four 1.5 mm diameter circular structures that were semi-enclosed in 600 µm thick SU-8 walls (Fig. S3*A*-*C*); this design was adapted from one reported previously[6] for other applications. Briefly, 2 mL SU8-2050 (MicroChem) was spin-coated at 2000 rpm for 30 seconds, followed by a soft-bake on a hotplate at 65°C for 3 minutes and 95°C for 8 minutes. The substrate was then exposed to UV light (11 mJ/cm^2 for 20 seconds) through a photomask and then post-baked at 65°C for 3 minutes and 95°C for 8 minutes and then immersed in SU8 developer for 8 minutes (MicroChem). The substrate was then hard-baked at 200°C on a hot plate for 5 minutes. As with all of the OET devices used in this study, wires were affixed to the top and bottom plates, and devices were assembled by joining a top and bottom plate together via a 150-µm-thick bio-compatible spacer (3M 9965) to form an enclosed chamber (Fig. S3*D*). The assembled device was then affixed to a standard microscope glass slide (Fig. S3*E*) and operated in the experimental setup as described previously[3,5] and in the main text. As indicated in Fig. S3*F* and *G*, the height of a representative micro-well wall was measured to be approximately 58 µm using an optical Profilometer (Bruker Contour GT-K).

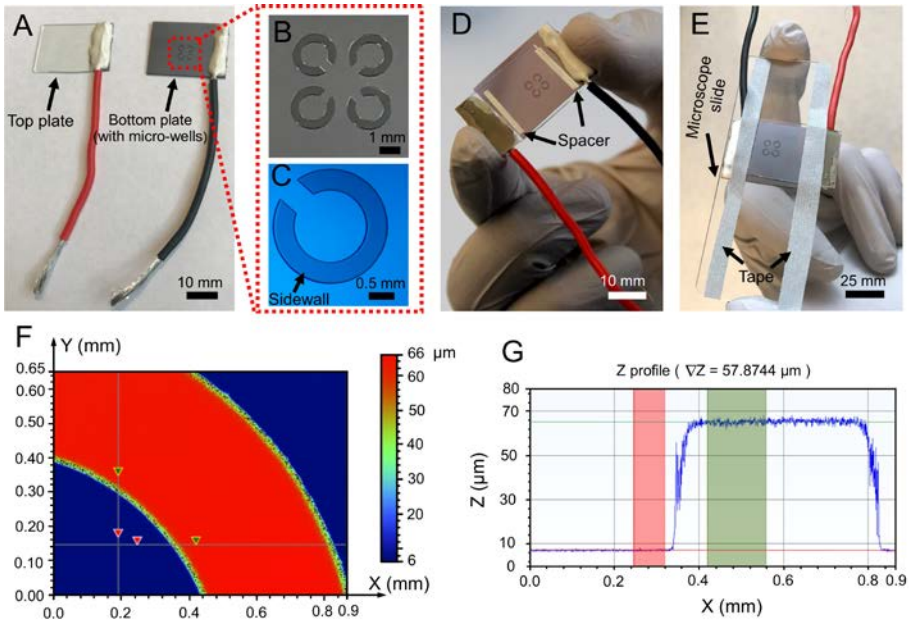

Fig. S3. Micro-well OET devices for clonal expansion and RNA-seq. (*A*) Picture of top plate and bottom plates (the latter bearing SU-8 micro-wells) of an OET device. (*B*) Close-up picture of micro-wells on the bottom plate. (*C*) Bright-field microscope image of a single micro-well. (*D*) Picture of an assembled OET device, with the two plates held together by the spacer. (*E*) Picture of an OET device affixed to a microscope slide with tape. (*F*) Height distribution (top view) for a portion of a representative micro-well wall, in which the height is indicated in a heat map (blue = low, red = high). (*G*) Cross-sectional profile of the micro-well's sidewall, indicating the sidewall has a height of approximately 58 µm.

The devices depicted in Fig. S3 were operated as described in the Methods section of the main text (for conventional OET devices) with a few changes. Devices were first loaded with 18 µL sucrose buffer containing microrobots. This volume fills approximately 90% of the chamber, including the spaces inside and outside of the micro-wells. Then, 2 µL of a mixture of suspended B-16 and U-87 cells that had been previously transfected[7] to express tdTomato and eGFP, respectively (a kind gift from Prof. Warren C. W. Chan, Univ. Toronto), was pipetted into one side of the chamber. When held flat and still, the cells were observed to settle in a small area at the edge of the OET device, while the remainder of the chamber (including the areas containing the micro-wells) remained cell-free (as depicted in Fig. 4*A* in the main text). OET was then used to manipulate a microrobot such that a targeted cell was loaded and then transported to a given microwell, where the cell was delivered. In replicate experiments, different cells (either B-16 or U-87) were delivered to different micro-wells. After loading single cells in the microwells, a paper tissue (Kimwipes, KIMTECH) was positioned at the edge of the chamber to wick the sucrose media out of the chamber, while fresh, pre-warmed (37ºC), serum-containing culture medium was dispensed by pipette at the other edge of the chamber. As described previously,[6] this arrangement of micro-wells was designed such that fluid in the center of the wells is not disturbed during this media-replacement step. For clonal expansion, devices were then stored in an incubator for up to 72 hours, periodically removing them for imaging. For RNA-seq analysis, devices were stored in an incubator for 12 hours, after which they were removed for analysis.

6. RNA-seq and Bioinformatics

Four samples were isolated using the microrobot system (as above): one B-16 cell, three B-16 cells, three U-87 cells, and five U-87 cells. After incubation for 12 hours, the cells were inspected by microscopy (Fig. S4*A*), the cell culture media was replaced with single-cell lysis buffer (Takara, 635013) including polyA-capture oligos [TTTTTTTAAGCAGTGGTATCAACGCAGAGTAC|CellBarcode(12bp)|UMI(8bp)|PolyT(30bp)], and the contents of each microwell was collected into a separate microcentrifuge tube. Using the Maxima H minus reverse transcriptase system (ThermoFisher) and a custom template-switching oligo (described previously[8]), cDNA was synthesized with an incubation of 30 min at 50ºC. The barcoded cDNA was then pooled and linearly amplified using SeqAmp DNA polymerase (Takara). A custom PCR handle[7] was used with the PCR cycles: 95ºC for 1 min, 18 cycles of 98ºC for 10 s, 65ºC for 30 s and 68ºC for 3 min, followed by a final 10 min extension at 72ºC. The cDNA was then purified and concentrated using Agencourt Ampure XP beads (Beckman Coulter, A63880) according to manufacturer's instructions, with a final elution in 10 μL of DEPC-treated water. The quantity and quality of cDNA was then assessed using an Agilent high sensitivity dsDNA kit (Agilent Technologies, 5067-4626) and a Qubit™ dsDNA HS Assay Kit (Invitrogen, Q32851). cDNA libraries were prepared for RNA-seq using the Nextera XT DNA library preparation kit (Illumina, FC-131-1096) according to the manufacturer's instructions with a final elution in 10 μL of DEPC -reated water. A custom P5 index sequence was used with standard P7 indices.[8] Libraries were sequenced on a MiSeq with the PE Miseq v3 reagent kit (Illumina) and with read sequencing lengths of 20bp for read1 and 130bp for read2, using a custom read1 primer.[8]

Raw RNA sequence data was pre-processed to identify and parse out the cell barcodes and unique molecular identifiers and to remove the sequencing adaptor sequences as well as any long stretches of polyA. The scripts for these steps can be found at https://github.com/eyscott and were adapted from a previous report.[8] Pre-processed fastq files were then aligned to their respective reference genomes: the Genome Reference Consortium Mouse Build 38 (for B-16 cells) and the Genome Reference Consortium Human Build 38 (for U-87 cells), with STAR (v2.5.3). The Rtsne package[9] was used perform t-distributed Stochastic Neighbor Embedding (TSNE) clustering (Fig. 4*G* in the main text) and Uniform Manifold Approximation and Projection[10] (UMAP) clustering (Fig. S4*B*), with visualization produced using the "ggplot2" R package.[11] Custom scripts developed for data analysis and visualization [including distributions of genes identified per sample (Fig. S4*C*) and read-counts per sample (Fig. 4*H* in the main text), and heat-map (Fig. 4*I* in the main text) and tabular form (Table S1) of the the subset of variable genes with S.E.M. > 30 for the four samples] can be found at https://github.com/eyscott.

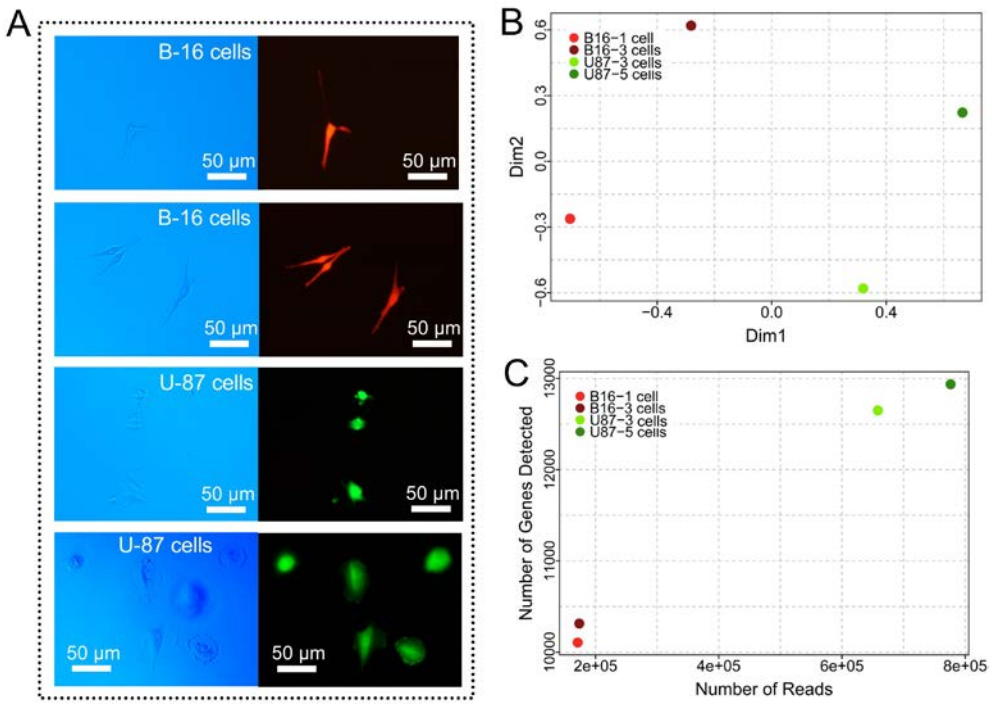

Fig. S4. Single- and small-cell-number RNA-seq. (*A*) Brightfield (left) and fluorescent (right) microscope images of one (top) and three (second-from-top) B-16 cells (red), and three (third-from-top) and five (bottom) U-87 cells (green) adhered to an OET device after selection, prior to analysis by RNA-seq. (*B*) Uniform Manifold Approximation and Projection (UMAP) dimensionality reduction of the transcriptome for each sample, for one (light red) or three (dark red) B-16 cells and three (light green) or five (dark green) U-87 cells, illustrating the large and small differences observed for the samples as a function of cell type and cell number, respectively. (*C*) Number of detected genes as a fucntion of the number of reads for the four samples. The clustering indicates that the number of detected genes per sample is largely impacted by the number of reads.

Table S1. Genes and corresponding expression values from Figure 4*I* in the main text.

Gene ID	1 B-16 Cell	3 B-16 Cells	3 U-87 Cells	5 U-87Cells
ACTB	521	479	746	608
ACTG1	1433	1439	2024	1800
ADM	1018	973	1441	1251
AKR1B1	552	579	883	746
ALDOA	713	695	1014	858
ANAPC11	269	292	429	354
ANXA1	526	506	815	664
ANXA2	1033	1062	1461	1312
ANXA5	370	328	537	476
AP2M1	232	271	369	332
ARF1	222	202	340	298
ARF4	206	209	335	288
ARPC2	213	219	358	313
ARPC3	292	283	477	362
ATOX1	226	225	373	308
ATP1B3	218	240	365	318
ATP5B	196	195	320	288
ATP5E	885	813	1238	1092
ATP5G2	277	295	456	375
ATP5J	276	294	474	385
ATP5O	231	245	401	332
ATP6V0B	265	250	402	339
ATP6V1G1	273	268	487	372
B2M	907	946	1376	1188
BAG3	407	423	640	495
BTF3	406	421	618	535
BUD31	290	281	413	374
CACYBP	176	165	305	247
CALM1	592	593	948	740
CALM2	574	582	885	739

CALU	576	596	892	718
CANX	260	256	399	327
CAV1	658	612	1005	853
CCT5	213	224	353	297
CCT6A	399	390	547	456
CD44	369	370	590	485
CD59	258	263	381	353
CD63	803	761	1132	988
CFL1	579	572	887	719
CHCHD2	570	601	847	764
CKS2	601	576	844	777
CLTA	626	612	907	763
COX4I1	620	614	947	869
COX5A	221	247	392	335
COX5B	427	387	604	542
COX6B1	384	409	682	573
COX6C	317	336	539	419
COX7C	374	399	610	461
COX8A	291	311	469	412
CSTB	452	428	654	581
CTC-425F1.4	84	66	261	120
CYCS	204	214	356	267
DDX5	315	332	478	421
DNAJA1	830	808	1210	1026
DNAJB1	385	366	615	507
DUSP1	326	344	565	431
EEF1A1	403	385	534	478
EEF1B2	354	323	532	456
EEF1D	480	474	693	630
EIF1	1064	1009	1559	1339
EIF4A2	201	192	337	277
EIF4G2	276	286	407	365
EIF5	359	410	616	489
EIF6	292	294	458	422
ELOC	330	350	493	445
ENO1	1208	1213	1718	1568
FAU	854	839	1258	1122
FTH1	2642	2607	3413	3163
FTL	2959	2946	3802	3535
GADD45B	615	620	923	798
GADD45GIP1	237	242	441	351
GAPDH	2685	2711	3565	3233
GAS5	310	297	468	414
GHITM	262	279	435	343
GNG11	169	196	319	231
GPX1	237	251	372	334
GSTP1	354	316	506	464
GUK1	250	272	416	366
H2AFZ	571	547	773	711
H3F3B	507	512	844	694
HERPUD1	379	421	626	546
HINT1	435	401	669	582
HMOX1	320	281	476	409
HNRNPA1	426	416	661	544
HNRNPA2B1	382	420	624	573
HSBP1	217	204	346	303
HSP90AA1	1317	1345	1973	1733
HSP90AB1	1089	1054	1566	1435
HSP90B1	334	301	536	444
HSPA5	608	526	828	713
HSPA8	680	655	972	870
HSPA9	193	198	308	295
HSPD1	357	330	510	440
HSPE1	387	366	569	474
IGFBP6	208	227	369	260
KCNMA1	289	284	458	403
KRT10	299	289	446	401
KRT81	762	738	1140	982
KTN1	298	248	458	362
LDHA	688	607	1003	877
LDHB	324	298	491	412
LGALS1	1649	1672	2342	2071
LMNA	307	275	438	371
LRRC75A-AS1	584	574	898	783
LSM3	283	270	440	342
LSM4	218	239	375	290
MAP1B	179	206	310	277
MGST1	316	382	535	484
MORF4L2	198	209	358	278
MRPL51	260	231	373	318
MT-ATP6	567	570	904	820
MT-CO1	502	543	813	743
MT-CO2	827	851	1217	1079
MT-CO3	314	292	488	416

MT-CYB	289	291	432	409
MT-ND1	515	484	750	683
MT-ND2	273	310	454	396
MT-ND4	732	757	1134	966
MT-RNR2	3070	3111	4022	3775
MT2A	1438	1467	2088	1814
MYL12A	241	245	403	318
MYL12B	460	442	638	573
MYL6	1159	1162	1698	1592
NACA	467	503	814	714
NAP1L1	203	183	323	243
NDUFA1	174	161	292	233
NDUFA11	167	170	294	257
NDUFA4	471	472	658	575
NDUFAB1	139	153	277	230
NDUFB2	424	387	614	581
NDUFB7	271	282	425	332
NDUFB9	287	278	450	425
NDUFS5	233	223	362	324
NENF	223	234	358	292
NPM1	655	591	911	798
NQO1	590	602	856	793
NUDC	291	263	442	364
OAZ1	785	786	1119	1035
P4HB	386	357	558	479
PARK7	280	271	406	402
PFDN5	512	517	798	658
PFN1	378	374	631	441
PGK1	201	217	339	273
PHLDA2	441	479	688	622
PKM	238	227	377	343
PLAU	1243	1255	1715	1555
PLAUR	263	229	369	319
PMAIP1	271	268	426	346
POMP	291	282	397	394
PPIA	613	623	924	842
PPIB	522	507	883	713
PPP1R14B	204	214	328	305
PRDX1	944	981	1376	1246
PRDX4	254	286	427	348
PSAP	331	306	470	393
PSMA7	1801	1758	2577	2169
PSMB1	311	306	446	388
PSMB3	345	327	534	441
PSMB6	403	378	620	558
PSMC5	242	199	348	287
PSMD2	227	240	424	350
PTGES3	342	368	539	460
PTMA	352	335	608	495
PTTG1	265	260	388	355
RAB31	247	269	377	351
RAC1	271	245	428	352
RACK1	761	785	1130	992
RAN	366	370	543	513
RBM3	235	214	398	325
RBX1	251	247	421	388
RHEB	170	197	307	257
RHOA	271	296	446	397
RHOC	454	446	703	581
RND3	316	301	432	419
ROMO1	303	290	446	418
RP11-713D19.1	444	436	654	590
RPL10	938	980	1425	1267
RPL10A	244	211	362	307
RPL11	1248	1331	1864	1650
RPL12	853	821	1262	1085
RPL13	1187	1221	1749	1541
RPL13A	776	768	1122	1001
RPL14	435	476	736	591
RPL15	549	549	837	671
RPL18	536	480	776	703
RPL18A	460	478	726	602
RPL19	1369	1339	1922	1745
RPL21	768	748	1178	998
RPL22L1	314	330	493	432
RPL23	507	530	776	686
RPL23A	601	661	968	839
RPL24	589	556	857	747
RPL26	649	668	984	879
RPL27	1042	1037	1516	1305
RPL27A	889	850	1305	1107
RPL28	307	304	451	384
RPL3	1203	1189	1724	1464
RPL30	1151	1234	1712	1533

RPL31	877	850	1292	1099
RPL32	917	1002	1471	1255
RPL34	409	447	689	588
RPL35	1041	1030	1503	1393
RPL35A	795	867	1283	1097
RPL36	272	303	442	413
RPL36A	229	212	359	239
RPL37	594	628	936	833
RPL37A	749	691	1054	891
RPL38	583	563	879	767
RPL39	377	377	585	475
RPL4	520	511	841	704
RPL41	292	310	501	419
RPL5	269	245	423	387
RPL6	563	550	783	744
RPL7	567	520	804	768
RPL7A	612	580	864	745
RPL8	1209	1212	1764	1548
RPL9	729	729	1111	982
RPLP0	1305	1313	1806	1638
RPLP1	2271	2295	3064	2742
RPLP2	1419	1480	2026	1855
RPN2	219	211	341	280
RPS11	318	297	472	386
RPS12	2280	2374	3093	2845
RPS13	992	1004	1437	1322
RPS14	1415	1420	1939	1721
RPS15	835	849	1201	1098
RPS15A	548	589	862	698
RPS16	1147	1120	1615	1493
RPS17	1190	1147	1677	1488
RPS18	659	597	964	815
RPS19	1439	1549	2078	1921
RPS2	1179	1090	1652	1480
RPS20	1374	1376	1925	1669
RPS21	1240	1208	1723	1533
RPS23	1125	1069	1644	1437
RPS24	651	597	959	785
RPS25	316	300	482	411
RPS27	1056	1011	1491	1275
RPS27A	1446	1430	2072	1786
RPS27L	402	424	629	516
RPS28	807	791	1218	1047
RPS29	473	453	736	633
RPS3	466	483	669	586
RPS3A	443	483	715	632
RPS4X	772	765	1175	997
RPS5	1042	1002	1465	1327
RPS6	1460	1515	2074	1922
RPS7	468	482	695	616
RPS8	781	803	1160	1008
RPS9	400	416	628	566
RPSA	815	836	1189	1071
RTN4	279	284	452	370
S100A10	1049	1014	1452	1248
S100A11	226	234	392	326
S100A6	2013	2071	2846	2529
SDCBP	175	163	294	243
SEC61B	220	223	360	309
SEC61G	225	243	392	321
SELENOK	245	239	386	323
SEM1	335	310	494	409
SERF2	566	525	802	718
SERP1	270	257	414	330
SERPINE1	339	323	482	449
SERTAD1	664	663	986	922
SH3BGRL3	887	852	1264	1124
SKP1	452	456	690	547
SLC25A5	357	320	508	453
SLC3A2	314	314	467	412
SLIRP	289	285	449	410
SNHG1	346	320	473	415
SNHG5	502	469	714	677
SNRPD2	316	312	483	425
SNRPE	173	158	296	234
SNU13	181	182	310	279
SNX3	334	325	519	444
SOD1	832	794	1255	1118
SON	237	200	413	281
SPANXB1	349	345	579	503
SPCS1	231	246	411	344
SQSTM1	579	572	847	757
SRP14	407	403	570	534
SRSF3	355	425	590	502

SSBP1	286	294	427	331
TBCB	409	386	613	533
TGFBI	814	774	1133	1005
TIMP1	300	315	474	404
TMA7	215	185	372	282
TMBIM6	320	339	516	426
TMEM258	217	215	356	323
TMSB10	2797	2855	3689	3430
TMSB4X	683	677	966	799
TNC	203	221	355	310
TPI1	973	944	1406	1255
TPM1	203	159	312	238
TPM3	214	242	361	317
TPT1	1684	1657	2359	2051
TSPO	390	338	565	451
TUBA1B	845	847	1224	1120
TUBB4B	432	396	601	544
TXN	660	718	1083	877
TXNDC17	212	244	348	300
TXNRD1	226	222	363	311
UBA52	753	724	981	909
UBB	587	636	935	784
UBC	1085	1055	1521	1323
UBE2C	260	242	398	318
UBL5	258	246	406	333
UCHL1	541	571	818	727
UPP1	291	300	420	395
UQCR10	310	294	472	415
UQCR11	279	302	482	384
UQCRB	315	300	475	401
UQCRH	394	390	586	503
UQCRQ	532	545	795	711
USMG5	447	448	658	592
VIM	2086	2151	2873	2512
WBSCR22	293	268	433	380
YWHAB	424	416	647	555
ZFAND2A	366	348	574	515
ZFAS1	757	729	1102	916

7. Cell-cell fusion

Devices used for cell-cell fusion were similar to the generic OET devices described in the main text, except that the top plate (bearing the unmodified ITO layer) was modified to include two 1 mm dia. inlet- and outlet-holes, and the spacer (150 μm thick) between the top and bottom plates featured a xurographic microfluidic channel formed by precisely cutting double-sided biomedical tape (3M 9965) with a craft cutter (Sihouette Cameo 3). The microfluidic channel consists of a main chamber (4.5 mm width, 27.5 mm length) connected to a narrow channel (0.5 mm width, 10 mm length). The sidewalls of the main chamber were designed to feature trapezoidal 'micro-docks' (roughly 500 μm deep, 800 μm wide at the opening, and 500 μm wide at the inner wall), used to collect targeted cells using the microrobot for subsequent study. Finally, PDMS reservoirs bearing two punched holes (4.5 mm dia. for the inlet and 1 mm dia. for the outlet) were formed using standard techniques[6,12,13] and affixed to the top of the top plates. The reservoirs were connected to PVC tubes (inlet: Tygon S3 B-44-3, inner dia. 1.6 mm; outlet: Tygon S-54-HL, inner dia. 0.25 mm), with the outlet tube interfaced to a programmable syringe pump (Harvard Apparatus PHD Ultra). (Note: all dimensions are given as-designed; the actual structures had some variation upon fabrication and assembly.)

In typical experiments, the microfluidic device (Fig. S5*A*) was mounted on a Peltier heater (Mouser Electronic, CP50441) at 37° C on the microscope (Fig. S5*B*). The system was operated with the syringe pump in withdraw mode, such that negative pressure drives the flow at a controllable rate. Prior to use, the channel was flushed with 100 μL PBS conaining 0.1% F-68 (ThermoFisher Scientific 24040032) (to block the surfaces), and then with 100 μL sucrose buffer, all at 15 μL/min.

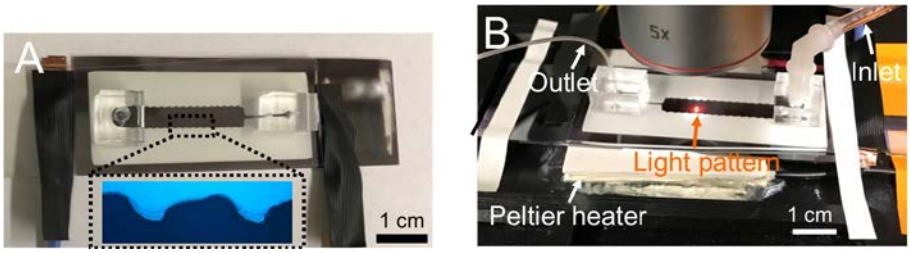

Fig. S5. Microfluidic device for cell fusion and selection from complex samples. (*A*) Photograph of an assembled microfluidic device. Inset (corresponding to dashed box in the main panel): bright-field microscope imag of two 'micro-docks' at the sidewall of the microchannel. (*B*) Image of the microfluidic device in operation. The device is positioned on a Peltier heater, with flow rate controlled via syringe pump connected to the outline (not shown).

Cell-fusion methods described previously[12-15] were adapted for use with microrobots. Briefly, suspensions of microrobots and mixed B-16 and U-87 cells (in sucrose buffer) were sequentially loaded into the microchannel via the syringe pump (20 μL and 30 μL, respectively, at 5 μL/min). OET was then used to drive microrobots to capture different combations of 2-3 cells, which were then driven into micro-docks at the edge of the channel. The channel was then flushed with 50 μL hypoosmotic buffer (Eppendorf 940002109) at 5 μL/min. Ten 40 V DC pulses (each 100 μs duration) were then applied between the top- and bottom-plate electrodes via a waveform generator (Agilent 33220A) connected to an amplifier (A.A. Lab Systems Ltd. 303), and the channel was flushed again with hypoosmolar buffer followed by supplemented DMEM (25 μL and 100 μL, respectively, at 5 μL/min). The device was then transferred to a humidified incubator filled with 5% (v/v) CO_2/air at 37ºC for 1 h, and then evaluated by fluorescence microscopy. The red/green fluorescent profiles in Fig. 5*C* (main text) were measured using ImageJ.

8. Selection of neurospheres from complex samples

Pimary neural dissections were collected from Oct4-GFP mice, which were maintained in the Department of Comparative Medicine at the University of Toronto in accordance with institutional guidelines (AUP 20011556). Briefly, mice were anesthetized with isoflurane (Fresenius-Kabi) followed by cervical dislocation on postnatal day eight. The brain was removed and the periventricular region was dissected. Tissue was digested with enzymes (1.33 mg/mL trypsin, 0.67 mg/mL hyaluronidase, and 0.2 mg/mL kynurenic acid) (Sigma-Aldrich) for 25 min at 37°C, as described previously.[16] Cells were centrifuged and samples were suspended in trypsin inhibitor (0.67 mg/mL, Worthington), mechanically dissociated into a single-cell suspension and plated at clonal density of 10 cells/μL[17] in serum-free media containing 1% penicillin/streptomycin (Invitrogen) supplemented with epidermal growth factor (20 ng/mL, Sigma-Aldrich), basic fibroblast growth factor (10 ng/mL, Sigma-Aldrich), and heparin (7.35 ng/mL, Sigma-Aldrich). After seven days, the sample (containing suspended neurospheres and other constituents) was centrifuged at 500×g for 5 min and resuspended in sucrose buffer prior to introduction into a standard OET device for manipulation. In OET experiments, 6 μL of sucrose buffer was loaded from one side of the device, and 8 μL each of neurosphere sample and microrobot suspension (in series) were loaded from the other side of the device. Designated neurospheres were identified, and as illustrated in

Movie S9, optoelectronic microrobots were steered around obstacles to collect the targeted neurospheres to bring them to the edge of the device for extraction by micropipette for futher culture and analysis.

9. Supplementary movie captions

Movie S1. A cogwheel-shaped microrobot is translated at 500 μm/s (clip 1) and then rotated at 6.28 rad/s (clip 2), 2.09 rad/s (clip 3) and 0.63 rad/s (clip 4).

Movie S2. A box-shaped microrobot is translated at 100 μm/s (clip 1) and then rotated at 0.63 rad/s (clip 2). A spaceship-shaped microrobot is translated at 300 μm/s (clip 3) and then rotated at 2.09 rad/s (clip 4).

Movie S3. A cogwheel-shaped microrobot is used to load, transport, and deliver one 15 μm diameter polystyrene bead (clip 1), and to load and transport three 15-μm-diameter polystyrene beads (clip 2).

Movie S4. Four cogwheel-shaped microrobots (with payloads of one or two 15-μm-diameter polystyrene beads) are simultaneously, repeatedly translated in different directions such that they exchange places (clip 1). Eight cogwheel-shaped microrobots are simultaneously rotated at different angular velocities (clip 2). Four cogwheel-shaped microrobots (with payloads of one, two, or three 15-μm-diameter polystyrene beads) are simultaneously translated in the same direction (clip 3).

Movie S5. Three square-shaped microrobots are simultaneously, repeatedly translated in different directions such that they exchange places (clip 1). Three square-shaped microrobots are simultaneously rotated at different angular velocities (clip 2). Four spaceship-shaped microrobots are simultaneously, repeatedly translated in different directions such that the exchange places (clip 3). Four spaceship-shaped microrobots are simultaneously rotated at different angular velocities (clip 4).

Movie S6. A cogwheel-shaped microrobot is used to load and transport two ARPE-19 cells (clip 1), to transport three MCF-7 cells (clip 2), and to transport five ARPE-19 cells (clip 3).

Movie S7. An OET light pattern is used to translate a single APRE-19 cell at 50 μm/s (clip 1), and a cogwheel-shaped microrobot is used to translate a single APRE-19 cell at 150 μm/s (clip 2).

Movie S8. Under an applied bias of 18 $V_{p\text{-}p}$ at 20 kHz, a circular OET projection is observed to induce rapid lysis on a series of MCF-7 cells (clip 1). When the same conditions are used to control a cogwheel-shaped microrobot, an MCF-7 cell is manipulated at 200 μm/s (clip 2).

Movie S9. Cogwheel-shaped microrobots are used to transport targeted neurospheres through a complex, heterogeneous sample (clips 1-2). A cogwheel-shaped microrobot and targeted neurosphere is extracted from the edge of the OET device using a pipette (clip 3-4).

10. Supplementary references

1. Neale SL, Mazilu M, Wilson JIB, Dholakia K, Krauss TF (2007) The resolution of optical traps created by light induced dielectrophoresis (LIDEP). *Opt Express* 15: 12619-12626.
2. Huang SB, et al. (2013) High-purity and label-free isolation of circulating tumor cells (CTCs) in a microfluidic platform by using optically-induced-dielectrophoretic (ODEP) force. *Lab Chip* 13, 1371-1383.
3. Zhang S, et al. (2018) Patterned Optoelectronic Tweezers: A New Scheme for Selecting, Moving, and Storing Dielectric Particles and Cells. *Small* 14: 1803342.
4. Jeorrett AH, et al. (2014) Optoelectronic tweezers system for single cell manipulation and fluorescence imaging of live immune cells. *Opt Express* 22: 1372-1380.
5. Zhang S, et al. (2018) Escape from an Optoelectronic Tweezer Trap: experimental results and simulations. *Opt Express* 26: 5300-5309.
6. Ke LY, et al. (2018) Cancer immunotherapy μ-environment LabChip: taking advantage of optoelectronic tweezers. *Lab Chip* 18: 106-114.
7. Chen YY, et al. (2016) Clarifying intact 3D tissues on a microfluidic chip for high-throughput structural analysis. *Proc. Natl. Acad. Sci. U.S.A.* 113: 14915-14920.
8. Macosko EZ, et al. (2015) Highly parallel genome-wide expression profiling of individual cells using nanoliter droplets. *Cell* 161: 1202-1214.
9. Krijthe JH (2015) Rtsne: T-distributed stochastic neighbor embedding using Barnes-Hu implementation. R package version 0.13, URL https://github. com/jkrijthe/Rtsne.
10. McInnes L, Healy J, Saul N, Großberger L (2018) UMAP: Uniform Manifold Approximation and Projection. *The Journal of Open Source Software* 3: 861.
11. Wickham H (2016) ggplot2: Elegant Graphics for Data Analysis. Springer-Verlag New York.
12. Hu N, Yang J, Joo SJ, Banerjee AN, Qian S (2013) Cell electrofusion in microfluidic devices: A review. *Sens Actuator B Chem* 178: 63–85.
13. Hsiao YC, Wang CH, Lee WB, Lee GB (2018) Automatic cell fusion via optically-induced dielectrophoresis and optically-induced locally-enhanced electric field on a microfluidic chip. *Biomicrofluidics* 12: 034108.
14. Dura B, Liu Y, Voldman J (2014) Deformability-based microfluidic cell pairing and fusion. *Lab Chip* 14: 2783-2790.
15. Skelley AM, Kirak O, Suh H, Jaenisch R, Voldman J (2009) Microfluidic control of cell pairing and fusion. *Nat Methods* 6: 147-152.
16. Sachewsky N, et al. (2014) Primitive neural stem cells in the adult mammalian brain give rise to GFAP-expressing neural stem cells. *Stem Cell Rep.* 2: 810-824.
17. Coles-Takabe BL, et al. (2008) Don't look: growing clonal versus nonclonal neural stem cell colonies. *Stem Cells* 26: 2938-2944.